where n_X is the refractive index for the crystalline state and n_A is the refractive index for the amorphous state. The optical spot sizes and signal contrasts of this medium have been described for several conditions.[20] The scattered electric fields in time domain snap shot of $x - z$ (at y=61Δ) and $y - z$ sectional plane (at x=61Δ) are shown in Figs. 5.4(a) and 5.4(b), respectively. The dimension of each cell are $\Delta x = \Delta y = \Delta z = \Delta$=5 nm, and the total space volume considered measures 121(x) ×121(y) ×151(z) cells. These results imply that the probe can work in the reflection detection mode because of the scattered electric fields from

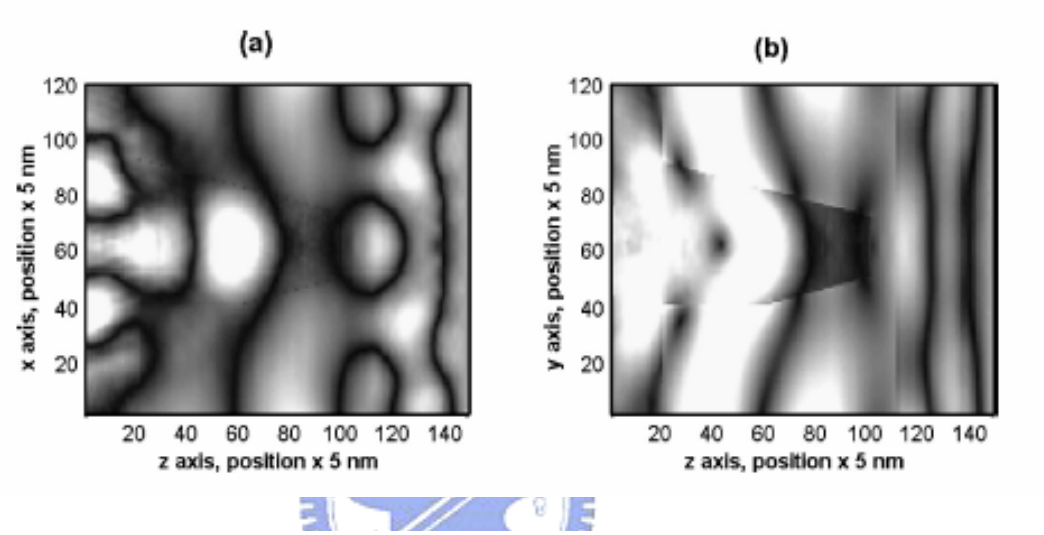

Fig. 5.4 The scattered electric fields in time domain snap shot of (a) $x - z$ (at y=61Δ) and (b) $y - z$ sectional plane (at x=61Δ), respectively.

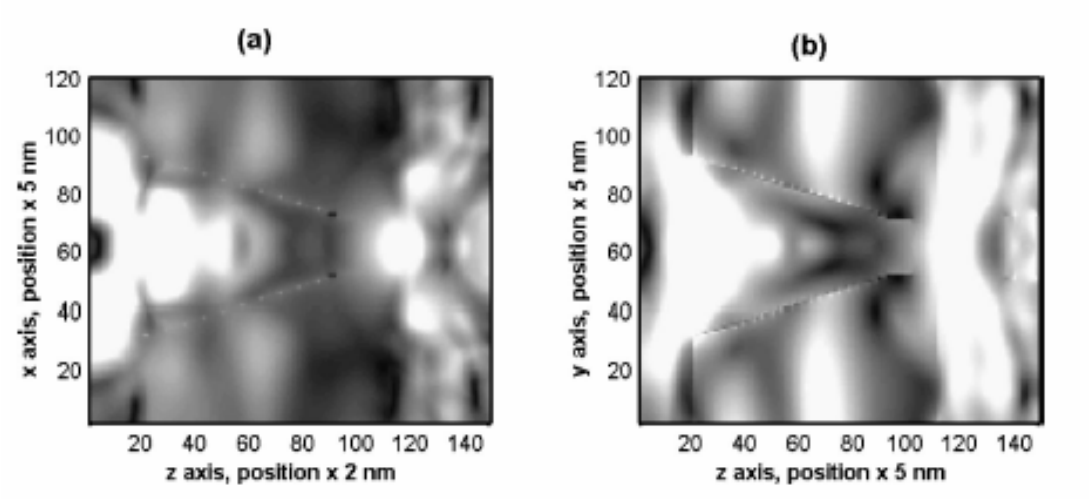

Fig. 5.5 The steady state electric field intensity plots of (a) the $x - z$ sectional plane and (b) $y - z$ sectional plane, respectively.

the recorded mark can propagate into the probe. The steady state of electric field intensity plots of the $x - z$ sectional plane and $y - z$ sectional plane are illustrated in Figs. 5.5(a) and 5.5(b), respectively. The beam diameter (in $1/e^2$ maximum intensity) in the $x - z$ and $y - z$ sectional plane directions at the inside of the recording layers is 220 and 150 nm, respectively. These sizes are smaller than the wavelength light λ =633 nm. The more detailed calculation using the 3D FDTD method is shown in Fig. 6, which illustrates the beam profile along x and y axis in the plane of z=5 nm, z=15 nm, z =25 nm from the exit surface of LaSFN9 glass probe, respectively. The results show that the outgoing light from the probe apex is weaker than that emitting from the lateral side and base of the SIL probe, and behaves as a strong contrast to the outgoing light of the probe apex. It implies that, for a dielectric SIL probe, propagating wave emitting from the intersection base of the SIL probe and from the conic side is stronger than that the outgoing light from the probe apex. It dominates the near-field distribution, while a film of metal is coated, the coated film can confine the light more strictly inside the probe tip and reduce the light of leakage from the SIL probe. The SIL-probe coated metallic film will provides a dramatic improvement in this regard. This will be understood in the Sec. 5.3.3.

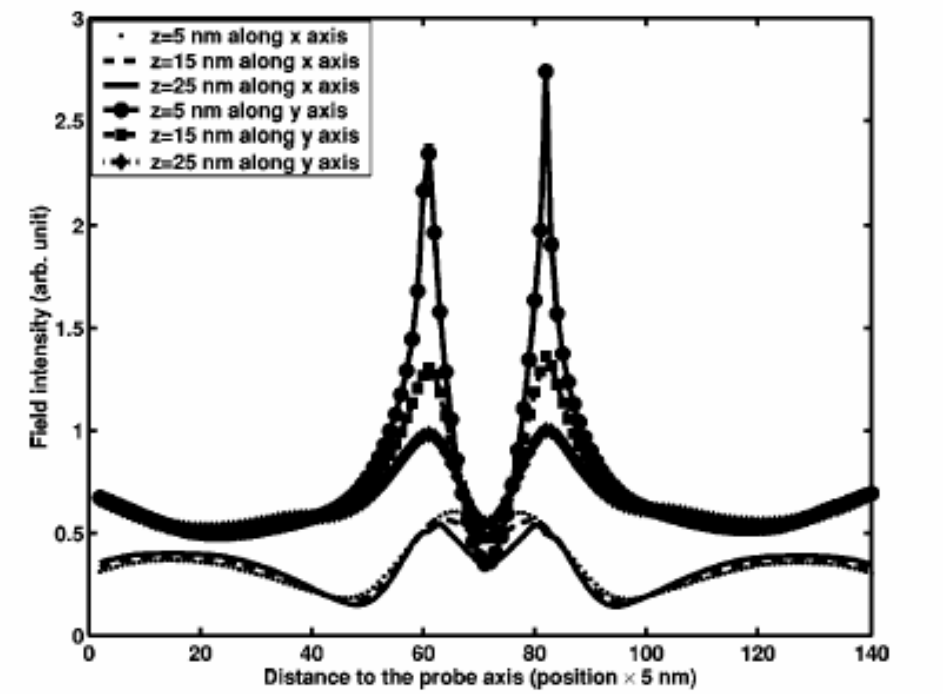

Fig. 5.6. Electric field distribution of the dielectric SIL probe along the x and y axis in the plane of z=5, 15, 25 nm, respectively.

5.3.3 A promising idea of fabricating a SIL-probe system

In the following, we will discuss one of the possible approaches and simulations about our idea of an optimal design of the SIL-probe system. It may be possible to fabricate a local metallic aperture in combination with a SIL. Experimental results show that the large background reflection from the metallic film that surrounds the apertures limit the detectable signal. Although the background reflection from the dielectric apertures is negligible, consider the aperture-only system where poor contrast is a result of the collection system not gathering enough spatial frequency information. Basically, laser light is focused by an objective lens onto a moving recording layer. The SIL probe which is in near contact with the recording layers, reduces the wavelength by a factor of *n (*refractive index of the SIL probe) and produces a small spot size. Reflected light is collected by the objective lens and directed to the detectors. The angular range of collected information is determined by the SIL probe, the objective lens, and the detector. If the angular range of collected information from the path between the recording layers and the SIL probe can be avoided by the light passing the metallic thin film, an optimal SIL probe with metallic film will be realized possibly. We can use both the advantage of high transmission efficiency with no absorption of the dielectric SIL probe and local enhancement of the metallic coating one (probe tip coated with metallic film which could be used to produce spots smaller than that generated with dielectric SIL-probe, but detection of the modulation is not efficient when uses it alone) to create a type of probe. Probe tips are fabricated directly on the bottom of a hemispherical SIL. The bottom face of SIL near to the entrance of probe is coated with aluminum film of 30 nm height with ring shape at the base of the SIL probe which external part and interior part are 480 and 300 nm, respectively. Detailed of the design and the fabrication process of dielectric aperture probe combined with the SIL are discussed in Refs. [21] and [22]. Fabrication of our improved SIL-probe system is illustrated as following steps: (1) mount SIL-probe in carrier; (2) coat with photoresist; (3) expose photoresist to cross-grating pattern; (4) develop photoresist; and (5) metal coating. In the process of coating the aluminum thin film, we keep the tip apex exposed to fabricate a local uncoated metal tip. That is to say, the probe is based on the metal probe and extends the internal dielectric material outside the metal probe. In order to avoid the large back background reflection from the metallic layer that surrounds the apertures limit the detectable signal, the length of the metallic coating must be short enough with the ratio to the SIL probe. So the background reflection from the metallic film in the reflection process can be neglected. Note that the incident light is accurately focused on the

central part of the SIL bottom. The ratio to the length between the metallic film and the noncoated part of the probe is approximately 2:1. The diameter of the probe apex, the large end of the probe, and the height of the probe are approximately 0.3 λ/n, 0.87 λ/n, 1.1 λ/n nm. The purpose of metallic coating is to conceal the lateral passing light and to enhance the field intensity locally inside the probe. Figure 7 shows a sectional diagram of a 3D FDTD model with recording layers of the improved probe to be analyzed. The dimension of each cell are $\Delta x = \Delta y = \Delta z = \Delta = 5$ nm, and the total space volume considered measures 141(x) ×141(y) ×151(z) cells.

Here, let us choose the coordinate of probe apex to be $x=71\Delta$, $y=71\Delta$, $z=101\Delta$. Figure 8 shows the linear gray scaled map of the total electric field modulus on the $x-z$ sectional plane (at $y=71\Delta$) and the $y-z$ sectional plane (at $x=71\Delta$) for y-polarization illumination, respectively. The scattered electric fields in time domain snap shot of $x-z$ (at $y=71\Delta$) and $y-z$ sectional plane (at $x=71\Delta$) are shown in Figs. 5.9(a) and 5.9(b), respectively. Figure 5.10 shows the electric field distribution of the local metallic coating SIL probe along the x and y axis in the plane of z=5, 15, 25 nm, respectively. Obviously, Fig. 5.10 compares with Fig. 5.6, the field intensity of improved probe is stronger than the dielectric probe at the border between dielectric and metal, but on the contrary at the center of the probe tip. We can regard the incident wave from the uncovered part of the improved SIL probe as the outgoing light passing through the dielectric one. This is to be expected since the propagating process in the uncovered part is similar to the dielectric SIL probe. In the sectional plane at $x=71\Delta$ ($y-z$ sectional plane), the light mainly escapes to the lateral side and has the strongest field intensity at the intersection place between dielectric and air. In the sectional plane at $y=71\Delta$ ($x-z$ sectional plane), the maximum distribution occurs along the z axis down to the probe tip.

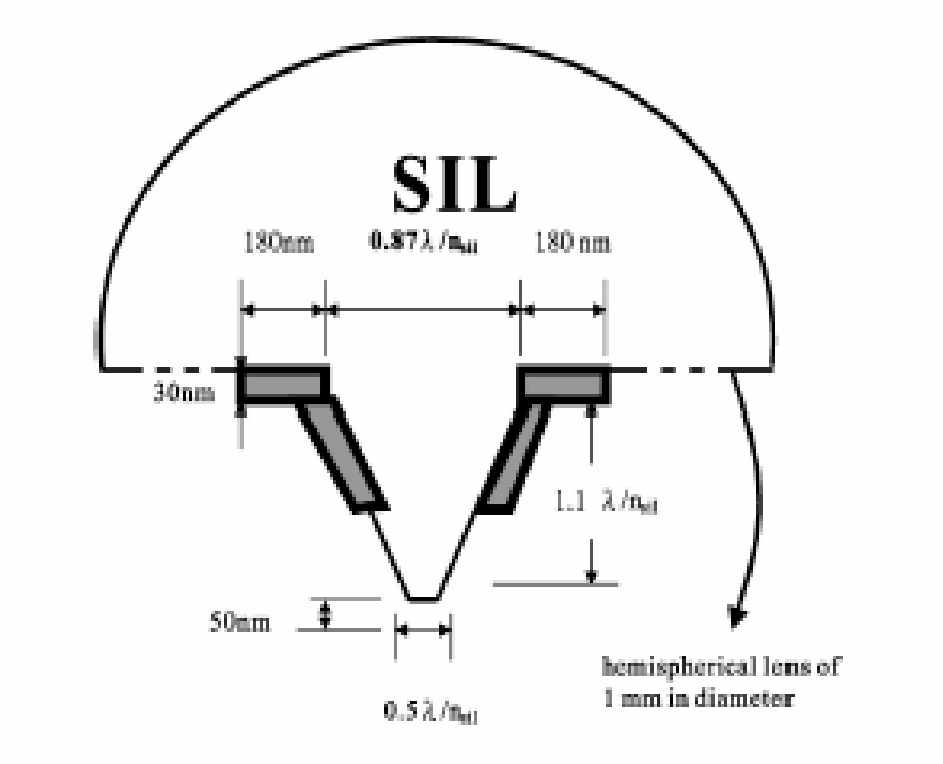

Fig. 5.7 The optimized geometry of the sectional diagram of the improved SIL-Probe system.

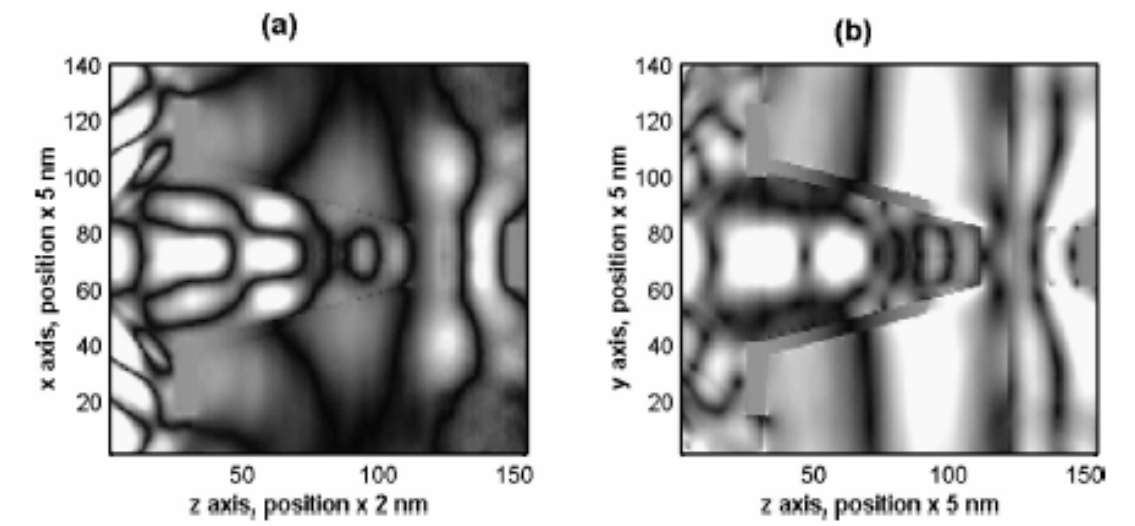

FIG. 5.8. The gray-scaled map of the total electric field modulus on the $x-z$ sectional plane (at y=71 Δ) and $y-z$ sectional plane (at x=71 Δ) for y-polarization illumination, respectively.

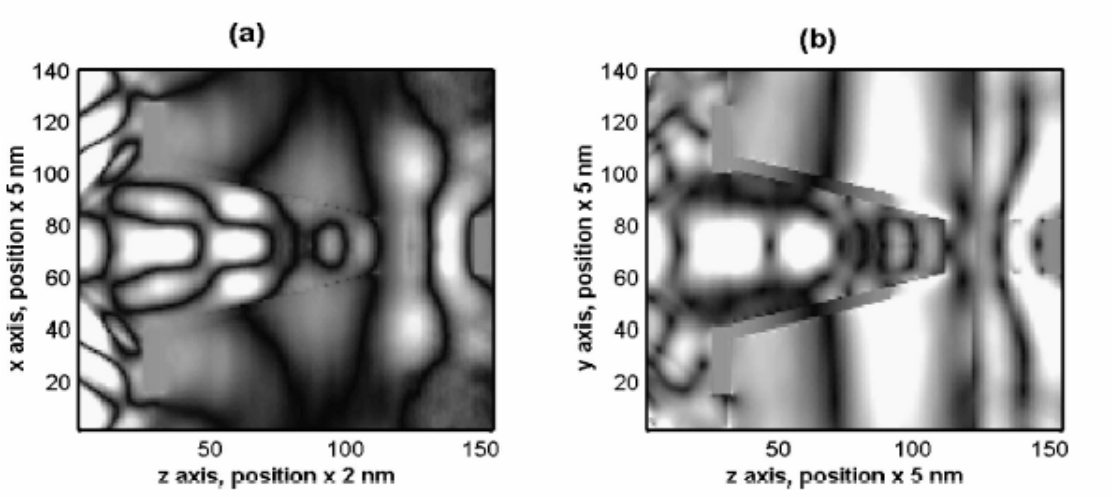

FIG. 5.9. The scattered electric fields in time domain snap shot of the $x - z$ (at $=71\Delta$) and $y - z$ sectional plane (at $x=71\Delta$) are shown in Figs. 5.8(a) and 5.8(b), respectively.

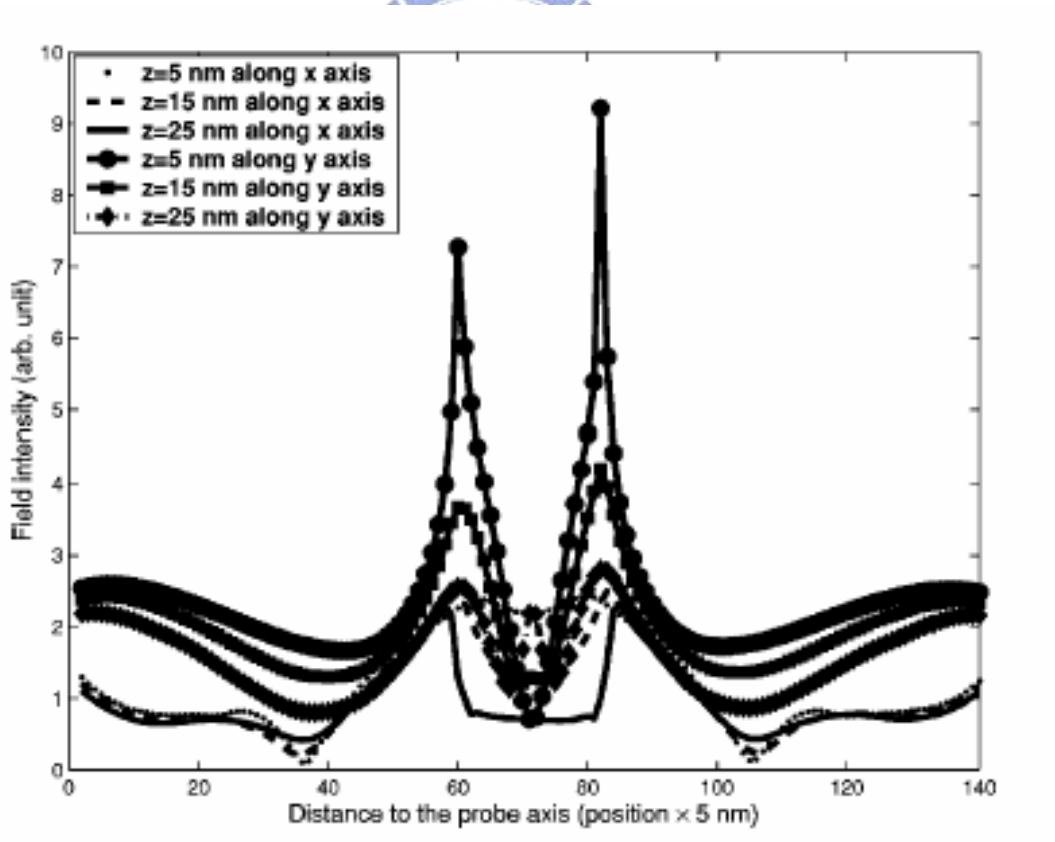

5.10. Electric field distribution of the local metallic coating SIL-probe along the x and y axis in the plane of z=5, 15, 25 nm, respectively.

5.4 Conclusion

In this article, we report a series of 3D FDTD simulations to obtain more insight in the mechanisms responsible for the SIL-probe system in NSOM architecture and a promising idea to fabricate an optimal SIL-probe system is proposed. It is found that the electric field leaking from the base and conic side of the SIL-probe system is much stronger than the output of the probe apex. Our optimal SIL-probe system shows that the local metallic coating on the base of the SIL and the lateral side of the probe demonstrate high throughput and low reflection of the light beam compared with the conventional metal NSOM probe used only. The beam size inside the recording-layers, using the case of LaSFN9 glass, is estimated to be smaller than (3/4) $\lambda / n_{\text{sil-probe}}$ (in $1/e^2$ maximum intensity). The computed field from the recording layers supports the hypothesis that the optimal SIL probe which we have designed can work in the reflection-detection mode. In the near future, we intend to consider other detailed effects involving, e.g., the influences of taper angles, probe diameter, refractive index of inner dielectric material of the SIL probe, the polarization, focus positions, and the nonlinear response of the irradiated recording layers.

References

[1] E. Betzig, J. Trautman, R. Wolfe, E. Gyorgy, P. Finn, M. Kryder and C. Chang: Appl. Phys. Lett. 61(1992) 142.

[2] Y. M.artin, S.Rishton and H. Wickramasinghe: Appl. Phys. Lett. 71(1997) 1

[3] F. Issiki, K. Ito, K. Etoh and S. Hosaka: Appl. Phys. Lett. 76(2000) 804

[4] T. Yatsui, M. Kourogi, K. Tsutsui, M. Ohtsu and J. Takahashi:Opt. Lett. 25 (2000)67

[5] H. Yoshikawa, Y. Andoh, M. Yamamoto, K. Fukuzawa, T. Tamamura and T. Ohkobo:Opt. Lett. 25(2000)1296

[6] B.D. Terris, H.J. Mamin and D.Rugar: Appl. Phys. Lett. 68(1995) 141.

[7] B.D. Terris, H.J. Mamin and D.Rugar: Appl. Phys. Lett. 65(1994)388.

[8] T. Milster, K. Shimura, J. Jo and K. Hirota: Opt. Lett.24(1999)605

[9] L. P. Ghislain and V. B. Elings: Appl. Phys. Lett.72(1998)2779.

[10] Kusato Hirota, Tom D Milster, Yan Zhang and J. Kevin Erwin, Jpn. J. Appl. Phys. Vol. 39(2000) pp.973-975

[11] A. Roberts: J. Appl. Phys. 65(1989)2896

[12] A. Roberts: J. Appl. Phys. 84(1998)6485

[13] R. Chang, P.K. Wei, W.S. Fann, M. Hayashi and S.H. Lin:J. Appl. Phys. 81(1997)3369

[14] R. Muller and C. Lienaa: Appl. Phys. Lett. 74(1995)976

[15] K. S.Yee. IEEE Trans. Antennas Propagat., 1966,AP-14:302-307

[16]A. Taflove, Computational Electrodynamics:The Finite-Difference Time-Domain Method , Norwood, MA, Artech House,1995.

[17] K. S. Kunz and R. J. Luebbers, The Finit Di®erence Time Domain Method for Electromagnetics, Boca, Raton, FL, CRC Press,1993

[18] H. Furukawa, S. Kawata, Optics Comm. 132(1996)170-178

[19] L. Novotny, D.W. Pohl and B. Hecht. Opt. Lett,20(9):970-972,1995.

[20] T. D. Milster, J. S. Jo, K. Hirota, K. Shimura, in digest of the International Symposium on Optical Memory, Tsukuba, 1998),paper Pd-15.

[21] Y.Zhang, K. Hirota, T. D. Milster and J. K. Erwin: Jpn. J. Appl. 39(2000) 973

[22] Tom D.Mister, Farhad Akhavan, Melissa Bailey, J. Kevin, David M. Felix, Kusato Hirota, Steven Koester , Kei Shimura AND Yan Zhang Jpn. J. Appl. Phys. Vol. 40(2001) pp. 1778-1782